ADVANCED FUNCTIONAL MATERIALS
www.afm-journal.de

Oligotriphenylene Nanofiber Sensors for Detection of Nitro-Based Explosives

Yao Zu Liao, Veronica Strong, Yue Wang, Xin-Gui Li, Xia Wang,* and Richard B. Kaner**

Blue light-emitting oligotriphenylene nanofibers are synthesized by oxidizing triphenylene using ferric chloride. By adjusting the monomer concentration, the acid used, and the temperature employed, the average diameter and length of the nanofibers can be readily tuned from 50 to 200 nm and 0.5 to 5 μm, respectively. Structural characterization, electrical conductivity, thermal stability, and fluorescence of oligotriphenylene, along with a proposed nanofiber formation mechanism, are presented. Both oligotriphenylene nanofiber dispersions and oligotriphenylene/polysulfone composite films are developed as fluorescent sensors for detecting traces of nitro-based explosives including nitromethane, nitrobenzene, and 2,4,6-trinitrophenol, as well as an electron-deficient metal ion, Fe(III). The sensors exhibit much better selectivity and sensitivity compared to conventional sensors, with detection limits down to 1.0 nM with a detection range covering ~4 orders of magnitude. The detection mechanism of the fluorescent sensors is also disscussed.

1. Introduction

One-dimensional (1D) π-conjugated nanosystems have received much attention as advanced electronic and photonic materials and devices.[1–4] Conjugated polycyclic aromatic hydrocarbons (PAHs) are well-known for exhibiting the ability to self-assembly into 1D nanostructures through strong π–π stacking interactions.[5–10] Triphenylene represents the smallest example of an all-benzenoid PAH,[11–13] and its derivatives exhibit unique electro/photoluminescence,[14,15] charge-carrier mobility,[16–18] energy migration,[19,20] and thermal and chemical stability.[21,22] Triphenylene-based materials have thus emerged as one of the leading candidates for the fabrication of low-dimensional electronic devices such as photoconductors,[16,23] light-emitting diodes,[21,22,24] and discotic liquid crystals.[25,26] In particular, oligotriphenylene has a long delocalized π–π conjugation, and is known to exhibit greatly enhanced electronic and photonic properties compared to the triphenylene monomer.[27] Interactions of oligotriphenylene with nitro-based compounds such as nitrobenzene (NB), dinitrobenzene (DNB), 2,4,6-trinitrotoluene (TNT), and 2,4,6-trinitrophenol (TNP) are also a subject of considerable interest. Note that TNP is an even more violent explosive than its well known counterpart TNT even at picomolar concentrations. The conjugated oligotriphenylene opens up the possibility of fabricating advanced sensors, which might find applications for readily detecting nitro-based explosives.

Oligotriphenylene was initially synthesized by electropolymerizing the triphenylene monomer.[27–30] Other triphenylene related copolymers or dendritic polymers have been synthesized using microwave-assisted Suzuki–Miyaura polymerizations[21,22,31] and Diels–Alder reactions.[32] However, simple routes to strong blue light-emitting oligotriphenylene nanofibers and attempts to develop them as sensors for the detection of nitro-based explosives have so far met with only limited success.

In this work, strong blue light-emitting oligotriphenylene nanofibers are readily synthesized by oxidizing triphenylene using ferric chloride ($FeCl_3$) without any templates, surfactants, or functional dopants. The nanostructures of oligotriphenylene can be readily tuned by controlling the monomer concentration, the acid used, and the temperature employed. Dedoped oligotriphenylene nanofibers exhibit good thermal stability, high fluorescence quantum yield, and stable fluorescence. The oligotriphenylene nanofibers are shown as effective fluorescent sensors for detecting nitro-based explosives such as nitrobenzene (NB), dinitrobenzene (DNB), and 2,4,6-trinitrophenol (TNP) as well as an electron-deficient metal ion, Fe(III).

2. Results and Discussion

2.1. Synthesis, Structure, and Morphology

The synthetic route, oligomerization mechanism, and proposed structure for oligotriphenylene are shown in **Scheme 1**.

Dr. Y. Z. Liao, Prof. X. Wang
School of Materials Science and Engineering
University of Shanghai for Science and Technology
516 Jun-Gong Road, Shanghai 200093, P. R. China
E-mail: wangxia@usst.edu.cn
Dr. Y. Z. Liao, V. Strong, Y. Wang, Prof. R. B. Kaner
Department of Chemistry and Biochemistry
University of California
Los Angeles, CA 90095-1569, USA
E-mail: kaner@chem.ucla.edu
Dr. Y. Z. Liao, Prof. X.-G. Li
College of Materials Science and Engineering
and Institute of Materials Chemistry
Tongji University
1239 Si-Ping Road, Shanghai 200092, P. R. China
E-mail: adamxgli@yahoo.com

DOI: 10.1002/adfm.201102013

© 2012 WILEY-VCH Verlag GmbH & Co. KGaA, Weinheim

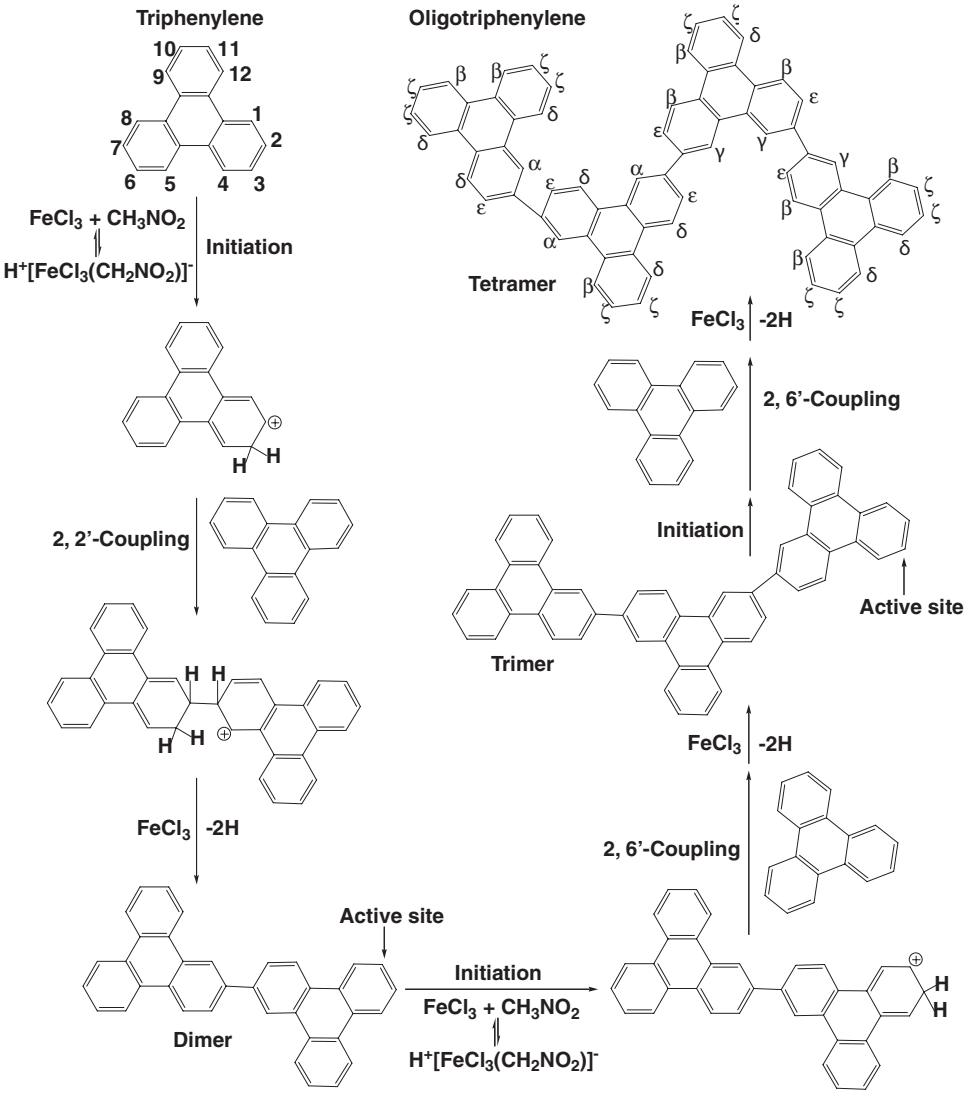

Scheme 1. Synthetic route and oligomerization mechanism to oligotriphenylene.

Structural analyses for oligotriphenylene were carried out by matrix-assisted laser desorption/ionization time-of-flight mass spectrometry (MALDI/TOF MS), ultraviolet-visible (UV–vis) spectroscopy, Fourier-transform infrared (FT-IR) spectroscopy, proton nuclear magnetic resonance (^{1}H NMR) spectroscopy, thermal analysis (TA), and elemental analysis (EA).

The UV–vis spectrum of triphenylene monomer shows weak absorptions at 320 and 335 nm owing to $S_0 \rightarrow S_3$ and π–π* transitions of an individual triphenylene moiety (**Figure 1**).[14,33–36] In contrast, the polymerized product, in addition to showing the π–π^* transition at 325 nm, also exhibits three new absorptions at 380, 405, and 435 nm, which can be attributed to the n–π^* transition of the bridged triphenylene moieties. This implies that extended π-conjugation of oligomers has been created by chemically oxidizing triphenylene. A MALDI/TOF mass spectrum of the product shows three typical peaks at 906.1, 680.3, and 454.5 g mol^{-1} with an average mass differential between adjacent peaks of 226 g mol^{-1} (Figure S1 in the Supporting Information). This indicates that the polymerization product has a limited molecular weight and consists of 2 to 4 triphenylene moieties, which make this material a collection of oligotriphenylene rather than polytriphenylene. Element analyses reveal the presence of C (91.62 wt%), N (0.05 wt%), and H (4.38 wt%) in oligotriphenylene. The C/H ratio is calculated to be 1.74. This

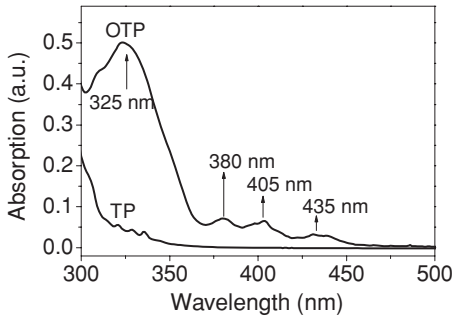

Figure 1. UV–vis spectra of triphenylene (TP) and dedoped oligotriphenylene (OTP) nanofibers dispersed in *N*-methyl-2-pyrrolidone (NMP).

© 2012 WILEY-VCH Verlag GmbH & Co. KGaA, Weinheim

value is consistent with the theoretical C/H ratio of the proposed oligotriphenylene (1.71), implying that the main chemical composition of the observed oligotriphenylene is $C_{72}H_{42}$. Additionally, an FT-IR spectrum of the triphenylene monomer exhibits three strong peaks near 619, 735 and 850 cm^{-1}, which can be attributed to the vibrations of four adjacent C–H bonds in the benzene rings (Supporting Information Figure S2).[37] These peaks visibly disappear or weaken in the oligotriphenylene spectrum as a result of dehydrogenation during oligomerization. Note that, two new peaks at 812 and 870 cm^{-1}, appear in the oligotriphenylene spectrum, which correspond to the vibrations of two adjacent C–H bonds in *para*-disubstituted benzene rings.[38–40] Additionally, both triphenylene and oligotriphenylene exhibit three peaks at 1431, 1496, and 1615 cm^{-1}, that represent vibrations of C=C and C–C bonds due to the presence of *ortho*-substituted benzene.[27] All this spectroscopic information signifies three types of C–H bonds: four-adjacent carbon-hydrogen, two-adjacent carbon-hydrogen, and one-adjacent carbon-hydrogen that make up the oligotriphenylene.

The protons in triphenylene at sites of 2, 3, 6, 7, 10, and 11 tend to possess a higher negative charge compared to protons found at other sites (i.e., 1, 4, 5, 8, 9, and 12),[27] and therefore they will be easier to initiate by an nucleophilic reagent, i.e. $FeCl_3$. Thus, oxidative polymerization will occur initially between 2- and 2′-carbon positions, and then 2- and 6′-carbon positions of the triphenylene monomer. This allows a chain to grow during the polymerization process leading to the formation of triphenylene dimer, trimer, and tetramer with a linear oligomeric chain structure, as illustrated in Scheme 1. This proposed mechanism is consistent with the MALDI/TOF mass spectrometry analysis. The chemical structures of the oligotriphenylene are further confirmed by using a ^1H NMR technique (Supporting Information Figure S3). The triphenylene monomer displays multiple peaks at 7.65–7.86 and 8.63–8.82 ppm, which can be attributed to the chemical shifts of protons at sites of 2, 3, 6, 7, 10, and 11, and 1, 4, 5, 8, 9, and 12, respectively. The oligotriphenylene shows a singlet peak at 9.12 ppm, a doublet peak at 8.90 ppm, a triplet peak at 8.86 ppm, a singlet peak at 8.82 ppm, a doublet peak at 8.75 ppm, and a doublet peak at 7.75 ppm, which can be attributed to the chemical shifts of H_α, H_β, H_γ, H_δ, H_ε, and H_ζ, respectively. In addition, the area of these peaks follows the ratio: 1: 3: 1: 3: 2: 4, confirming that the real chemical composition of oligotriphenylene is very similar to the proposed structure. The generation of oligotriphenylene can also be confirmed by thermal stability and conductivity measurements. The significantly enhanced electronic properties (~10^{-3} S cm^{-1} versus <10^{-10} S cm^{-1}, after doping with iodine vapor) and thermal stability (26% char yield versus 2% char yield, after heating at 1100 °C, Supporting Information Figure S4) of oligotriphenylene compared to triphenylene are most likely related to the formation of an extended π-conjugation.

The morphology of as-synthesized oligotriphenylene can be tuned from 3D aggregates to 2D nanosheets, to 1D nanofibers by controlling the following reaction parameters: the monomer molar concentration, the acid used, and the temperature employed, as shown by both scanning electron microscopy (SEM) and transmission electron microscopy (TEM). The quality and uniformity of the nanofibers are especially sensitive to the monomer molar concentration. Basically, low monomer molar concentrations (0.01–0.04 M) preferentially yield bulk quantities of nanofibers (**Figure 2**a,b). Nanofibers with diameters of <50 nm were produced when a 0.01 M monomer concentration was used (Figure 2a). When the monomer concentration was increased to 0.08 M, the nanofibers formed flake-like sheets with a thickness of <100 nm (Figure 2c). When the monomer concentration was further increased to 1.0 M, nanofiber formation was completely suppressed and the morphology became large sheets (Figure 2d). The quality of the

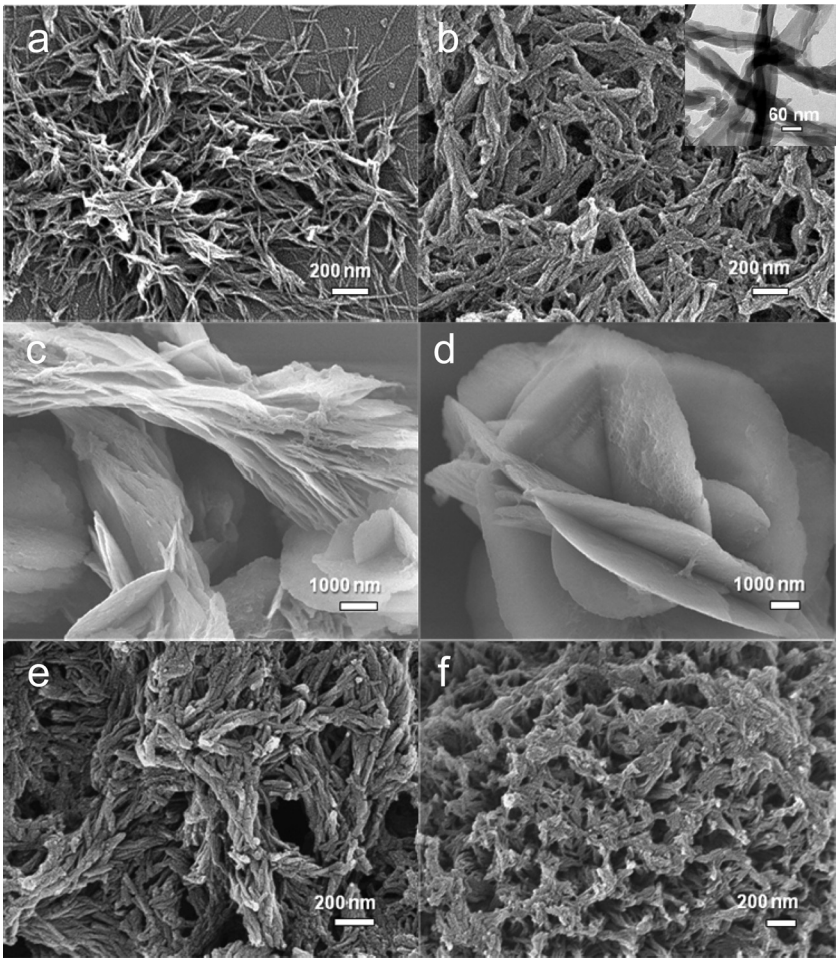

Figure 2. a–d) SEM images of oligotriphenylene synthesized with the following monomer concentrations: a) 0.01 M, b) 0.04 M, c) 0.08 M, and d) 1.0 M at room temperature; e–f) SEM images of the nanofibers synthesized at (e) 50 °C and (f) 60 °C with the same monomer concentration 0.01 M. The inset in (b) shows a TEM image of the oligotriphenylene nanofibers.

© 2012 WILEY-VCH Verlag GmbH & Co. KGaA, Weinheim

nanofibers thus depends on the monomer molar concentration, which is consistent with the results from a dilute polymerization method to make polyaniline nanofibers.[41,42] During dilute polymerization, a large amount of oligotriphenylene was able to be continuously deposited onto the active nuclei leading to bulk quantities of nanofibers. This is in contrast to the polymerization using a high concentration of monomer in which a large number of oligomers readily form and precipitate, followed immediately by secondary growth leading to sheets.

The temperature and the doping acid used also play significant roles in the synthesis of oligotriphenylene and can therefore also be used to control the nanofibrillar morphology. When the oligomerization temperature was increased from room temperature to 50 °C and then further increased to 60 °C, a large amount of agglomerated nanofibrillar structures are produced (Figure 2e,f). Although, nanofibrillar structures will form regardless of the doping acid used, the chosen acids such as camphorsulfonic acid (CSA), methanesulfonic acid (CH_3SO_3H), and trifluoromethanesulfonic acid (CF_3SO_3H) have a significant influence on the morphology. For example, CSA enhances the alignment and length of the oligotriphenylene nanofibers up to ~5 μm with diameters of ~200 nm (Supporting Information Figure S5). When the oligomers are doped with an acid, the oligomeric chains become protonated and the negatively charged dopant anions reside near the positively charged oligomers due to ionic attractions. The size and charge density of the doping acids thus influence the interchain packing distance and ultimately the supramolecular morphology. This explains why the oligotriphenylene exhibits dopant-induced nanoscale controllability.

2.2. Formation Mechanism of Oligotriphenylene Nanofibers

In order to more fully understand the formation mechanism for oligotriphenylene nanofibers, an investigation into the crystallinity of triphenylene and oligotriphenylene was carried out (**Figure 3**a). A powder X-ray diffraction (XRD) pattern of the triphenylene monomer shows several sharp peaks at Bragg angles 2θ of 8.6, 13.5, 17.3, 21.0, and 25.9°. The diffraction pattern of dedoped oligotriphenylene nanofibers exhibit three strong peaks at 2θ = 12.0, 21.2, and 26.4°. When compared to triphenylene, it appears that the oligotriphenylene nanofibers form a new ordered polycrystalline arrangement. Note the sharp new peak of oligotriphenylene at 2θ = 26.4°, which is essentially absent in the triphenylene and can be attributed to the oligomeric molecular π–π stacking with a *d*-spacing of 3.97 Å.

The existence of lamellar π–π stacking in oligotriphenylene is confirmed by both high resolution TEM and a fast Fourier transform (FFT) pattern. The FFT pattern of oligotriphenylene nanofibers demonstrates four diffraction rings and a clearly delineated six-fold symmetry (Figure 3b). This suggests a polycrystalline oligomer arranged in a planar orientation. A high-resolution TEM image of a single nanofiber shows typical lattice fringes due to the oligotriphenylene molecular stacking (Figure 3c). Previous studies on PAHs such as pentacene,[5] perylene,[6–9] and coronene[10] derivatives as well as conjugated polymers/oligomers such as polythiophene,[43] polyphenylene,[44] and oligo(*p*-phenylenevinylene)[45] have shown similar 1D nanostructures made by self-assembly resulting from strong π–π stacking between packed molecules. Analogously, the self-assembly along the π–π stacking direction with a *d* spacing of 3.97 Å, is believed to be the dominant driving force for the growth of 1D oligotriphenylene nanofibers.

2.3. Fluorescence and Sensors

When a UV lamp excites oligotriphenylene nanofibers dispersed in *N*-methyl-2-pyrrolidone (NMP), a highly visible and stable blue background photoluminescence appears. The blue photoluminescence is completely stable in air and can be sustained for at least six months. The fluorescence spectrum of oligotriphenylene nanofibers shows a maximum emission band at λ_{max} = 436 nm, and several additional bands at λ = 422, 445, and 462 nm, as well as a remarkable long-wavelength tail that ends at ~600 nm (**Figure 4**), thus fulfilling the requirements for a blue light-emitting polymer. The fluorescence intensity of the oligotriphenylene nanofibers is ~7 times stronger than that of the triphenylene monomer. After oligomerization, both maximum excitation and emission wavelengths of the oligotriphenylene nanofibers red shift by 92 and 71 nm, respectively, due to the extended conjugation length. Fluorescence quantum yield (Φ) of the oligotriphenylene nanofibers in solution can be calculated using the following equation:[46]

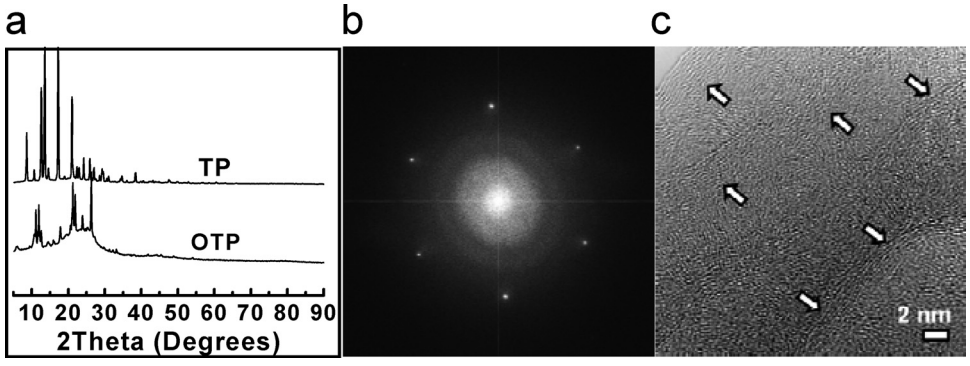

Figure 3. a) X-ray diffraction (XRD) patterns of triphenylene (TP) and dedoped oligotriphenylene (OTP) nanofibers. b,c) A fast Fourier-transform (FFT) pattern (b) and a high-resolution TEM image (c) of a single oligotriphenylene nanofiber. The arrows in (c) indicate the lattice fringes from the nanofiber.

© 2012 WILEY-VCH Verlag GmbH & Co. KGaA, Weinheim

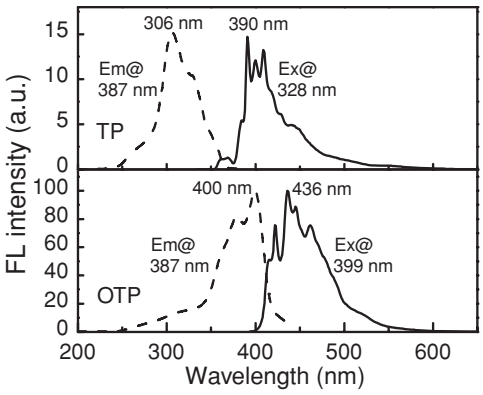

Figure 4. Excitation and emission fluorescence (FL) spectra of triphenylene (TP) monomer and dedoped oligotriphenylene (OTP) nanofiber dispersion at a concentration of 0.1 g L^{-1}.

$$\Phi = n^2 A_{ref} . I \Phi_{ref} ./ \left(n_{ref}^2 AI\right) \quad (1)$$

where n is the refractive index of the solvent, A is the absorbance at the excited wavelength, and I is the integrated area of emission. Triphenylene with a Φ value of 0.08–0.09,[47–49] was used as a reference material and NMP was used as the solvent for both triphenylene and oligotriphenylene. The fluorescence quantum yield of oligotriphenylene nanofibers is calculated to be ~0.5, which is more than 5 times that of the triphenylene monomer.

To make use of the excellent fluorescent properties of oligotriphenylene nanofibers, photoluminescent composite films were prepared by making a blend with polysulfone. The influence of different oligotriphenylene weight compositions, i.e., 0.3, 0.8, 1.5, and 4.5 wt% (relative to polysulfone), on the transparency and photoluminescence of the as-prepared composite films were investigated. Yellow solutions consisting of a mixture of oligotriphenylene nanofibers and polysulfone were found to exhibit strong blue light emission when excited by a UV lamp (**Figure 5**a). Highly transparent thin composite films were prepared by dipping the glass slides into the yellow solutions and then drying at 50 °C overnight. The composite films display transparencies of >75% in the visible region (Figure 5d). The composite films show a prominent fluorescence peak at 450 nm accompanied by three shoulder peaks at 433, 475, and 525 nm. Upon increasing the amount of oligotriphenylene in the composition, the fluorescence becomes stronger with the highest transparency occurring when 0.8 wt% oligotriphenylene was used (Figure 5b–e). Note that the prominent emission peak of the composite film has a 14 nm red shift compared to that of oligotriphenylene nanofiber dispersion. This is likely due to the oligotriphenylene chains in the film exhibiting more linear configurations with longer conjugation lengths. However, the half width of the emission spectra of the film and the dispersion are quite close (85 nm versus 82 nm), indicating that weak chain aggregations exist in the solid film,[50] and that oligotriphenylene is well dispersed in the polysulfone matrix.

Rapid detection of trace amounts of nitro-based explosives is crucial for environmental cleaning, military operations, homeland security, and humanitarian efforts.[51,52] Oligotriphenylene nanofibers have now been demonstrated to show high fluorescence quantum yield in dispersion and favorable emission properties in the solid state. Fluorescent conjugated polymers with extended aromatic systems are known to be excellent electron donors.[53] Their donor ability can be further enhanced when irradiated by a photon such as UV light due to their delocalized π^* excited states.[54] Electron-deficient chemicals, in particular, nitro-based explosives such as nitrobenzene (NB), dinitrobenzene (DNB), 2,4-dinitrotoluene (DNT), 2,4,6-trinitrotoluene (TNT), and 2,4,6-trinitrophenol (TNP), can act as electron acceptors for photo-excited electrons from the oligotriphenylene leading to a rapid and amplified fluorescence quenching. With this in mind, both dispersions and composite films of oligotriphenylene nanofibers were examined for their ability to detect nitro-based explosives as well as metal cations at trace concentrations, by characterizing the fluorescence quenching efficiency upon addition of the quenchers.

When 1.0×10^{-3} M concentrations of the nitro-based explosives including nitromethane (NM), nitrobenzene (NB), and 2,4,6-trinitrophenol (TNP) were added to the oligotriphenylene nanofiber dispersions, the photoluminescence intensity decreased markedly as is evident by comparison to the

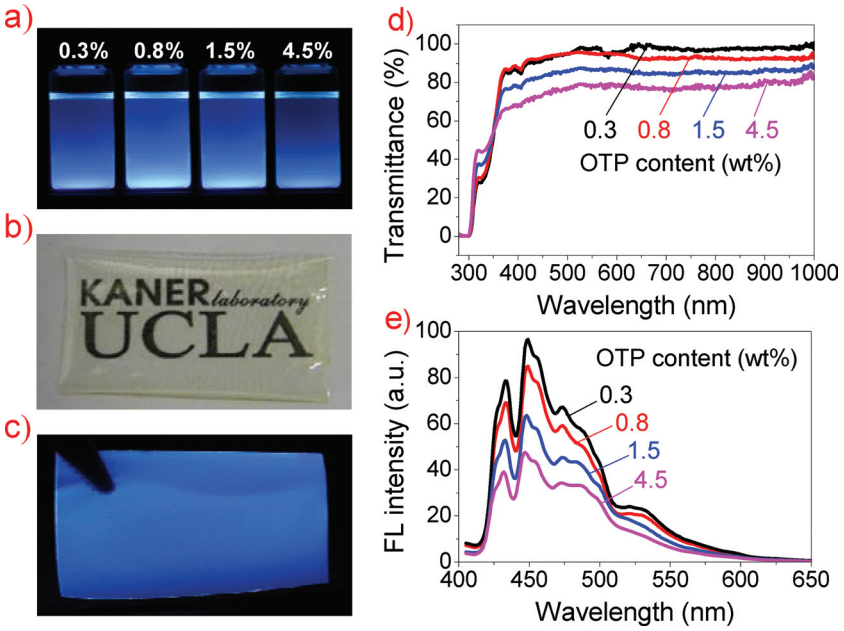

Figure 5. a) Blue light emission from NMP solutions of oligotriphenylene (OTP)/polysulfone (PSF) composites prepared with the following weight compositions of OTP relative to PSF: 0.3, 0.8, 1.5, and 4.5 wt%. A typical transparent thin film of an oligotriphenylene/polysulfone composite with 0.8 wt% composition of oligotriphenylene excited by sun-light (b) and UV light (365 nm) (c). d,e) Transmittance (d) and emission fluorescence (FL) (e) spectra of oligotriphenylene/polysulfone composite films prepared with different compositions of oligotriphenylene after excitation at 399 nm.

© 2012 WILEY-VCH Verlag GmbH & Co. KGaA, Weinheim

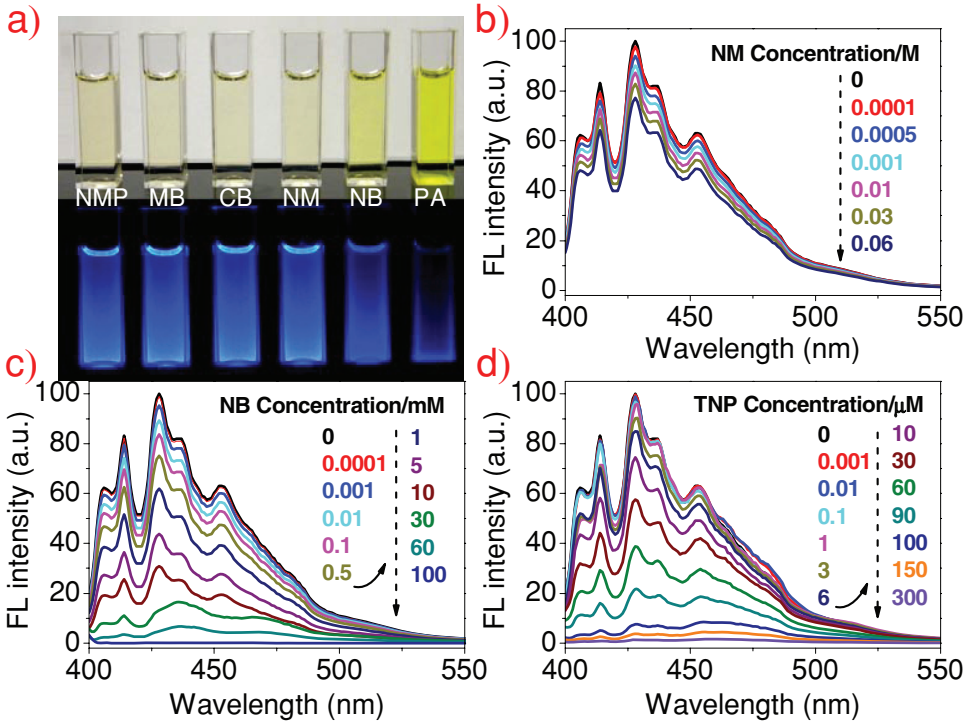

Figure 6. a) Photographs of 3 mL oligotriphenylene NMP dispersions (0.1 g L^{-1}) in a glass cuvette excited by sun-light and UV light (365 nm) after the addition of 0.2 mL of the following analytes (1.0×10^{-3} M) dissolved in NMP: methylbenzene (MB), chlorobenzene (CB), nitromethane (NM), nitrobenzene (NB), and 2,4,6-trinitrophenol (TNP), the photographs were taken with a high resolution advanced camera using UV–vis light filters. Concentration-dependent fluorescence (FL) quenching of an oligotriphenylene NMP dispersion (0.1 g L^{-1}) excited at 399 nm after adding different concentrations of nitromethane (NM) (b), nitrobenzene (NB) (c), and 2,4,6-trinitrophenol (TNP) (c).

negligible effects of adding reference materials such as methylbenzene (MB) or chlorobenzene (CB) (**Figure 6**a). The fluorescence spectral responses of oligotriphenylene to NM, NB, and TNP in NMP are shown in Figure 6b–d. The emission fluorescence intensity progressively decreased with an increase in the concentrations of the quenchers. On the basis of fluorescence titration, the limits of detection for NM, NB, and TNP using an oligotriphenylene dispersion are 1.0×10^{-4}, 1.0×10^{-7}, and 1.0×10^{-9} M, respectively. The quenching behavior is characterized by the quenching efficiency (F/F_0) and the quenching constant (K_{SV}) as determined by the Stern–Volmer equation:[54]

$$F_0/F = 1 + K_{SV}[Q] \quad (2)$$

where F_0 is the initial fluorescence intensity maximum without a quencher, F is the fluorescence intensity maximum with an added quencher of concentration [Q], and K_{SV} is the quenching constant.

Oligotriphenylene dispersions exhibit different photoluminescence quenching efficiencies ($Q_e = F_0/F–1$) for NM, NB, and TNP. The smallest $1/(Q_e + 1)$ value is observed when TNP is used, while values of 1 are found when the reference materials are added (**Figure 7**a). This implies that the quenching efficiency of oligotriphenylene follows the order: TNP >> NB >> NM > CB = MB. Thus, the oligotriphenylene sensors have a high selectivity for different nitro-based explosives resulting in widely varying responses. The quenching constants (K_{SV}) of oligotriphenylene dispersion sensors calculated from the linear part of the Stern–Volmer plots are 4.5×10^1 M^{-1} for NM, 1.9×10^2 M^{-1} for NB, and 2.8×10^4 M^{-1} for TNP (Figure 7b–d). Both the detection limit and the K_{SV} values for NB and TNP are comparable to values reported for the useful, but costly, polymers:

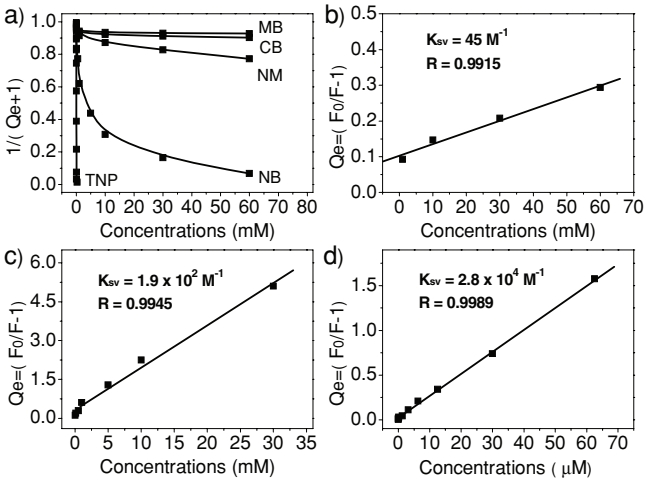

Figure 7. a) Fluorescence quenching efficiency (Q_e) (F_0/F –1) of oligotriphenylene sensors towards the following analytes: methylbenzene (MB), chlorobenzene (CB), nitromethane (NM), nitrobenzene (NB), and 2,4,6-trinitrophenol (TNP). (b–d) Stern–Volmer plots of oligotriphenylene sensors with the following analytes: b) NM, c) NB, and d) TNP.

© 2012 WILEY-VCH Verlag GmbH & Co. KGaA, Weinheim

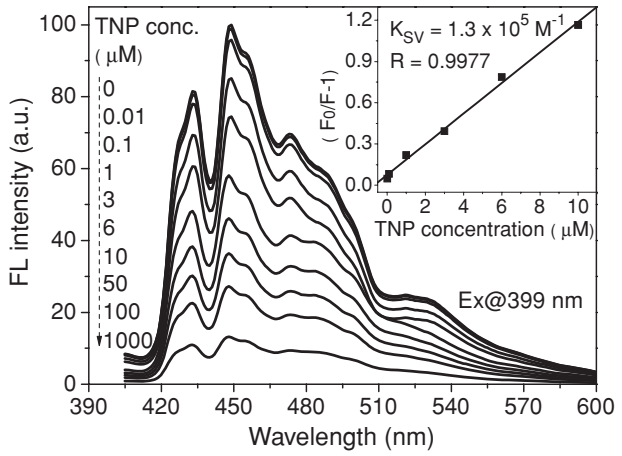

Figure 8. Concentration-dependent fluorescence (FL) quenching of oligotriphenylene/polysulfone composite films by the addition of different concentrations of 2,4,6-trinitrophenol (TNP) in DI water. The top right inset shows a Stern–Volmer plot of the oligotriphenylene film sensor.

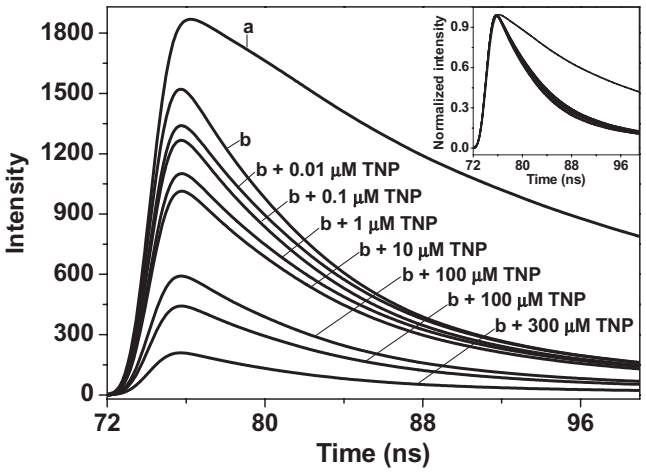

Figure 9. Time-dependent fluorescence decay data of oligotriphenylene in *N*-methyl-2-pyrrolidone (NMP) dispersions at concentrations of 3.1×10^{-4} g mL^{-1} (a) and 3.1×10^{-7} g mL^{-1} (b) and upon addition of trinitrophenol (TNP) NMP solutions at the following concentrations: 0, 0.01, 0.1, 1, 10, 100, 150 and 300 μM. The top-right inset shows the normalized time-dependent fluorescence decay data.

polymetalloles,[55] hydrosilylated poly(vinylene)s,[56] and polysiloles.[57] Note that the linear detection range of 2,4,6-trinitrophenol covers ~4 orders of magnitude of concentrations from 1.0×10^{-9} to 6.0×10^{-5} M.

Strongly photoluminescent oligotriphenylene/polysulfone composite films were also developed for the rapid detection of TNP in aqueous solution. Compared to oligotriphenylene dispersion sensors, film sensors can be recycled and are solvent-free, leading to a more convenient and environmentally friendly detection method. The fluorescence response of the composite film to TNP is shown in **Figure 8**. The fluorescence intensity decreases monotonically with an increase in the concentrations of TNP; the limit of detection is 1.0×10^{-8} M based on a fluorescence titration. From the linear part of the Stern–Volmer plot, the quenching constant (K_{SV}) is calculated to be 1.3×10^5 M^{-1}. Relatively less interaction exists between the film and the analyte, which may explain why the film sensors exhibit a lower sensitivity, compared to the dispersion sensors (1.0×10^{-8} M versus 1.0×10^{-9} M). However, the limited interactions may lead to a certain quenching mechanism, i.e., either a static process or a dynamic process, resulting in a relative higher quenching constant (1.3×10^5 M^{-1} versus 2.8×10^4 M^{-1}). Another important aspect of the sensors is their relative insensitivity to interferents. Control experiments in which aqueous inorganic acids including 0.5 M hydrochloric acid, sulfuric acid, and nitric acid were added into the aqueous TNP solutions produced negligible changes in the photoluminescence of the films (Supporting Information Figure S6). This signifies that the as-prepared sensors possess good selectivity toward TNP among the nitro-based compounds investigated.

Additionally, upon introduction of the same concentration (30 μM) of metal cations: K(I), Ca(II), Mg(II), Al(III), Zn(II), Cr(III), Cu(II), Fe(III), Ag(I), and Hg(II) into the oligotriphenylene dispersion (0.1 g L^{-1}), the fluorescence intensity was decreased markedly by Fe(III) in comparison to negligible changes observed with the other metal cations (Supporting Information Figure S7a). According to the fluorescence spectra (Figure S7b), the quenching efficiencies of K(I), Ca(II), Mg(II), Al(III), Zn(II), Cr(III), Cu(II), Fe(III), Ag(I), and Hg(II), are calculated to be 0.02, 0.04, 0.07, 0.06, 0.08, 0.07, 0.08, 0.92, 0.07, and 0.05 (Figure S7c), respectively. These results imply that the oligotriphenylene could be used as an Fe(III)-selective sensor with high sensitivity.

2.4. Detection Mechanism

In order to elucidate the detection mechanism of the sensors, the fluorescence lifetimes of oligotriphenylene NMP dispersions in the absence and presence of TNP were measured. The fluorescence lifetimes were calculated by fitting the time-dependent fluorescence decay data (**Figure 9**) to a single-exponential decay using the equation:

$$I(t) = I_0 e^{-t/\tau} \quad (3)$$

where $I(t)$ is the fluorescence intensity at time (t), I_0 is the initial fluorescence intensity, and τ is the fluorescence lifetime. The oligotriphenylene dispersion at a concentration of 3.1×10^{-4} g mL^{-1} has a fluorescence lifetime of 26 ns, which decreases to 9.2 ns when diluted to a concentration of 3.1×10^{-7} g mL^{-1}. This may be due to a large amount of NMP overshadowing the fluorescence of the oligotriphenylene. When 0.01, 0.1, 1, 10, 100, and 150 μM of TNP were added into 3.1×10^{-7} g mL^{-1} of an oligotriphenylene dispersions (9.2 ns), the lifetimes of the sensors were 10.1, 9.3, 9.2, 10.3, 9.0, 8.9, 10.0, and 10.1 ns (Figure 9, inset), respectively. The fluorescence lifetimes of the sensors remained almost unchanged upon addition of TNP. In contrast, the fluorescence intensity of the sensors largely depends on the concentrations of TNP, as shown in Figure 9. Clearly, the addition of TNP decreases the fluorescence yield, but has no change on the fluorescence lifetime of the oligotriphenylene. The sensors and TNP thereby appear to form a nonfluorescent complex in a ground state through a static quenching

© 2012 WILEY-VCH Verlag GmbH & Co. KGaA, Weinheim

interaction.[58] In addition, by multiplying the Stern–Volmer constant and fluorescence lifetime,[59] the quenching rate constant (K_q) of the sensors for TNP is calculated to be 2.6×10^5 ns M^{-1}. Such a high K_q further implies that the static quenching process is dominant in the oligotriphenylene sensors.

For conjugated polymer fluorescent sensors, Swager et al.[54] proposed that binding one receptor site results in an efficient quenching of all emitting units in an entire conjugated polymeric molecule. This amplification, known as the "molecular wire" effect, leads to electron donors and acceptors forming π-electron or charge transfer complexes between the oligotriphenylenes and their quenchers, as shown in **Scheme 2**a. The stereo structure generated by the above mentioned protocol was subjected to a molecular dynamics simulation using Chem3D Ultra8.0 software, which identifies the most probable minimum energy conformation (Scheme 2b). The results indicate that the oligotriphenylene forms a spiral-like architecture. This unique structure could readily capture electron-deficient analytes forming stable static complexes. We therefore believe that a static quenching process is dominant for the oligotriphenylene sensors through formation of a charge-transfer complex between the fluorophores and electron-deficient compounds. Note that, (1) charge densities (D) follow the order: $D_{Fe(III)}$ (6.09) > $D_{Al(III)}$ (5.40) >> $D_{Cr(III)}$ (3.08) > $D_{Ni(II)}$ (1.45) > $D_{Cu(II)}$ (1.28) > $D_{Zn(II)}$ (1.18) > $D_{Ca(II)}$ (0.40) > $D_{Hg(II)}$ (0.36) > $D_{Ag(I)}$ (0.12) > $D_{K(I)}$ (0.10) (the calculation for charge density is given in the supporting information), and standard potentials (ϕ) follow the order: $\phi_{Hg(II)}$ (0.85 V) > $\phi_{Ag(I)}$ (0.80 V) > $\phi_{Fe(III)}$ (0.77 V) > $\phi_{Cu(II)}$ (0.34 V) >> $\phi_{Cr(III)}$ (–0.41 V) > $\phi_{Zn(II)}$ (–0.76 V) > $\phi_{Al(III)}$ (–1.66 V) > $\phi_{Mg(II)}$ (–2.36 V) > $\phi_{Ca(II)}$ (–2.87 V) > $\phi_{K(I)}$ (–2.93 V),[59] implying that (1) Fe(III) is the most electron-deficient ion and possesses the highest electron-affinity; and (2) the paramagnetic property of Fe(III) with unpaired d electrons (d^5) provides additional metal-centered electrons, orbitals, and charge-transfer bands that can provide nonradiative decay pathways for the excited state of fluorophores.[60,61] Both effects lead to the formation of the more stable π-electron-metal complexes between Fe(III)'s and the oligotriphenylene oligomeric chains. This may explain why the oligotriphenylene sensors exhibit the most sensitivity and selectivity towards Fe(III).

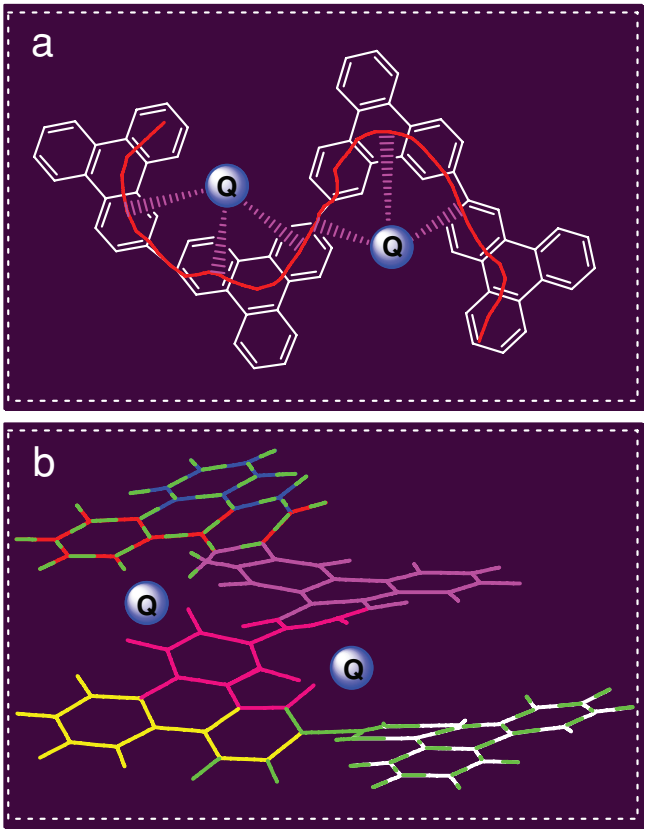

Scheme 2. a) A model of the π-electron transfer complex believed to be formed between the oligotriphenylene and quenchers (Q, blue balls), where the red solidline and magnenta dotted line represent the "molecular wire" pathway for transfer of the π-electrons; b) the 3D model of the above complex near the minimal energy state as found using Chem3D Ultra8.0 software.

3. Conclusions

Blue light-emitting spiral-like oligotriphenylene nanofibers have been readily synthesized using $FeCl_3$ as the oxidant without any templates, surfactants, or functional dopants. By controlling the monomer concentration, the doping acid used, and the reaction temperature employed, the average diameter and length of the nanofibers can be tuned from 50 to 200 nm and 0.5 to 5 μm, respectively. Strong π–π stacking of oligotriphenylene molecules produces the driving force for growth of the nanofibers. Conjugated oligotriphenylene nanofibers exhibit multifunctionality including good thermal stability, high fluorescence quantum yield, and stable fluorescence. Fluorescent sensors based on both dispersions and composite films of oligotriphenylene nanofibers enable the trace detection of nitro-based explosives including nitromethane, nitrobenzene, and 2,4,6-trinitrophenol as well as Fe(III). The Stern–Volmer constant (K_{SV}) values for the dispersion sensors are 4.5×10^1 M^{-1} for nitromethane, 1.9×10^2 M^{-1} for nitrobenzene, and 2.8×10^4 M^{-1} for 2,4,6-trinitrophenol. Thin film sensors demonstrate very high sensitivity and selectivity for 2,4,6-trinitrophenol in aqueous solution with a detection limit as low as 1.0×10^{-8} M and a K_{SV} as high as 1.3×10^5 M^{-1}. Fluorescence lifetime and UV-vis absorption measurements together with molecular dynamic simulations indicate that, the static quenching process is dominant for the oligotriphenylene sensors through formation of a charge-transfer complex between the fluorophores and electron-deficient compounds. Oligotriphenylene sensors therefore hold promise for use in environmental cleaning, military operations, homeland security, and humanitarian efforts due to their high sensitivity, good selectivity, and easy operation.

4. Experimental Section

Materials: All chemicals including triphenylene and polysulfone beads (M_n ~22,000) were purchased from Sigma–Aldrich and used as received. All the analytes including methylbenzene (MB), chlorobenzene (CB), nitromethane (NM), nitrobenzene (NB), 2,4,6-trinitrophenol (TNP) used in this work were analytical grade.

Synthesis of Oligotriphenylene Nanofibers: In a typical synthesis of oligotriphenylene nanofibers, 0.5 mmol of triphenylene was dissolved in

© 2012 WILEY-VCH Verlag GmbH & Co. KGaA, Weinheim

50 mL of dichloromethane, while 10 mmol of anhydrous ferric chloride ($FeCl_3$) as the oxidant was dissolved in 75 mL of nitromethane. The two solutions were rapidly mixed and shaken for ~15 s. The reaction was then sonicated for 30 min and further magnetically stirred for two days. Upon mixing of the monomer and oxidant solutions, the colorless monomer solution turned dark-brown. During sonication, the viscosity of the reaction system slowly increased and cotton-like solids precipitated out. After several hours of stirring, the viscosity decreased and uniformly dispersed fine particles were observed in the reaction solution. Finally, as-made nanofibers (in situ doped by $FeCl_3$) were obtained after purification by centrifugation using nitromethane. Dedoped nanofibers with a 72% yield were obtained by further washing the as-made nanofibers with 0.1 M hydrochloric acid, 0.1 M ammonium hydroxide, and finally DI water.

Preparation of Oligotriphenylene/Polysulfone Composite Films: The oligotriphenylene nanofibers and polysulfone beads were dissolved in NMP by magnetic stirring at 50 °C, forming composite solutions with different oligotriphenylene compositions (0.3, 0.8, 1.5, and 4.5 wt%). These solutions were then drop-cast onto glass slides and heated at 50 °C overnight to remove the solvents and produce transparent films.

Instrumentation and Measurements: Samples for field emission SEM (JEOL JSM-6700) were prepared on silicon wafers. Samples for TEM (PHILIPS CM120) were prepared on Formvar-coated copper grids (Ted-Pella). FFT patterns were obtained by directing the incident electron beam perpendicular to a single nanofiber. UV–vis absorption spectra of the monomer and polymer nanofibers dispersed in NMP were recorded on an HP 8453 spectrometer. Solid state FT-IR spectra of the samples as KBr pellets were carried out on a JASCO FT/IR-420 spectrometer. Powder XRD patterns were scanned on a Philips X'pert Pro spectrometer using copper-monochromatized CuKα radiation ($\lambda = 1.54178$ Å). The molecular weights of the oligotriphenylene nanofibers were determined using a Voyager DE MALDI-TOF spectrometer with dihydroxybenzoic acid as the matrix. Proton (^{1}H) NMR spectra were obtained using a Bruker ARX-400 spectrometer with $CDCl_3$ as the solvent. The C/N/H compositions of the oligotriphenylene were characterized by elemental analysis (EA) performed by Columbia Analytical Services, Inc.. Thermogravimetric analysis/differential thermogravimetric analysis (TGA/DTGA) scans were carried out on a Perkin Elmer TGA Pyris 1 by heating the samples from room temperature to 1100 °C at a rate of 10 °C min^{-1}. The fluorescence spectra of oligotriphenylene nanofiber dispersions and composite films were acquired on a PTI 3200 fluorescence spectrometer using a cuvette holder. For thin film measurements, each glass slide with the composite deposited on top was cut into an optimal dimension which can just fit into a 3 cm × 5 cm cuvette. Solution fluorescence quenching was performed by sequentially adding 0.2 mL of different analytes including NM, NB, TNP, MB, CB, K(I), Ca(II), Mg(II), Al(III), Zn(II), Cr(III), Cu(II), Fe(III), Ag(I), and Hg(II) to 3 mL of an oligotriphenylene NMP dispersion (0.1 g L^{-1}). The fluorescence lifetime measurements were carried out under the control of FeliX32 software from the Easylife X filter based lifetime system. ***Caution***: *2,4,6-trinitrophenol (TNP, known as picric acid) is an even more violent explosive than 2,4,6-trinitrotoluene (TNT) even at picomolar concentrations. It is very sensitive to heat and also forms shock sensitive compounds with heavy metals. It should be handled only in small quantities.* Film fluorescence quenching was carried out by fitting a glass slide with a composite film into a cuvette and then adding 3.2 mL of a TNP aqueous solution.The fluorescence spectrum was obtained after the film had soaked in the solution for ~10 min. The glass slide was cleaned by MilliQ water at least 3 times before carrying out fluorescence measurements.

To investigate electrical conductivity, dedoped oligotriphenylene nanofibers were redoped in iodine vapor at 60 °C for two days. The conductivities of sheet-like oligotriphenylene powders were measured using a two-point probe method.[62]

Supporting Information

Supporting Information is available from the Wiley Online Library or from the author.

Acknowledgements

This article was amended on February 22, 2012 to include the inset in Figure 2b, which was missing in the version originally published online. Y.Z.L. and V.S. contributed equally to this work. The authors thank Dr. Qihai Xu for help with ^{1}H NMR analyses. Financial support from Abraxis Bioscience (RBK), the China Scholarship Council No. 2008626064 (YZL), the Starting Fund from the University of Shanghai for Science and Technology (10-00-310-001), the National Science Foundation Graduate Research Fellowship (YW), Key Project of Science and Technology of Shanghai Commission (No. 10JC1411700), and the National Natural Science Foundation of China (No. 50873077) are gratefully acknowledged.

Received: August 24, 2011
Published online: December 14, 2011

[1] H. D. Tran, D. Li, R. B. Kaner, *Adv. Mater.* **2009**, *21*, 1487.
[2] F. J. M. Hoeben, P. Jonkheijm, E. W. Meijer, A. P. H. J. Schenning, *Chem. Rev.* **2005**, *105*, 1491.
[3] Y. Z. Liao, C. Zhang, X. Wang, X. G. Li, S. J. Ippolito, K. Kalantar-zadeh, R. B. Kaner, *J. Phys. Chem. C* **2011**, *115*, 16187.
[4] Y. Z. Liao, C. Zhang, Y. Zhang, V. Strong, J. S. Tang, X. G. Li, K. Kalantar-zadeh, E. M. V. Hoek, K. L. Wang, R. B. Kaner, *Nano Lett.* **2011**, *11*, 954.
[5] A. L. Briseno, S. C. B. Mannsfeld, X. M. Lu, Y. J. S. Xiong, A. Jenekhe, Z. N. Bao, Y. N. Xia, *Nano Lett.* **2007**, *7*, 668.
[6] A. L. Briseno, S. C. B. Mannsfeld, C. Reese, J. M. Hancock, Y. J. Xiong, S. A. Jenekhe, Z. N. Bao, Y. N. Xia, *Nano Lett.* **2007**, *7*, 2847.
[7] Y. K. Che, X. M. Yang, K. Balakrishnan, J. M. Zuo, L. Zang, *Chem. Mater.* **2009**, *21*, 2930.
[8] Y. Liu, K. R. Wang, D. S. Guo, B. P. Jiang, *Adv. Funct. Mater.* **2009**, *19*, 2230.
[9] A. F. Thünemann, D. Ruppelt, C. Burger, K. Müllen, *J. Mater. Chem.* **2000**, *10*, 1325.
[10] A. J. Fleming, J. N. Coleman, A. B. Dalton, A. Fechtenkötter, M. D. Watson, K. Müllen, H. J. Byrne, W. J. Blau, *J. Phys. Chem. B* **2003**, *107*, 37.
[11] M. D. Watson, A. Fechtenkotter, K. Müllen, *Chem. Rev.* **2001**, *101*, 1267.
[12] O. Lemaire, M. De Backer, A. Devos, F. X. Sauvage, *Synth. Met.* **2001**, *123*, 61.
[13] J. J. Schneider, D. Wolf, C. W. Lehmann, *Inorg. Chim. Acta* **2003**, *350*, 625.
[14] V. Duzhko, H. F. Shi, K. D. Singer, *Langmuir* **2006**, *22*, 7947.
[15] H. X. Mao, Z. Q. He, J. L. Wang, C. X. Zhang, P. Xie, R. B. Zhang, *J. Lumin.* **2007**, *122/123*, 942.
[16] D. Adam, P. Schuhmacher, J. Simmerer, L. Häussling, K. Siemensmeyer, K. H. Etzbach, H. Ringsdorf, D. Haarer, *Nature* **1994**, *371*, 141.
[17] D. Adam, F. Closs, T. Frey, D. Funhoff, D. Haarer, H. Ringsdorf, P. Schumacher, K. Siemensmeyer, *Phys. Rev. Lett.* **1993**, *70*, 457.
[18] A. Bayer, S. Zimmermann, J. H. Wendorff, *Mol. Cryst. Liq. Cryst. Sci.* **2003**, *396*, 1.
[19] D. Markovitsi, F. Rigaut, M. Mouallem, *Chem. Phys. Lett.* **1987**, *135*, 236.
[20] F. M. Mulder, J. Stride, S. J. Picken, P. H. J. Kouwer, M. P. De Haas, L. D. A. Siebbeles, G. J. Kearley, *J. Am. Chem. Soc.* **2003**, *125*, 3860.
[21] R. Kwong, B. Alleyne, *US Patent 0280965 A1*, **2006**.
[22] M. Saleh, Y. S. Park, M. Baumgarten, J. J. Kim, K. Müllen, *Macromol. Rapid Comm.* **2009**, *30*, 1279.
[23] J. Simmerer, B. Glüsen, W. Paulus, A. Kettner, P. Schuhmacher, D. Adam, K.-H. Etzbach, K. Siemensmeyer, J. H. Wendorff, H. Ringsdorf, D. Haarer, *Adv. Mater.* **1996**, *8*, 815.

© 2012 WILEY-VCH Verlag GmbH & Co. KGaA, Weinheim

[24] R. Freudenmann, B. Behnisch, M. Hanack, *J. Mater. Chem.* **2001**, *11*, 1618.
[25] S. Kumar, *Liq. Cryst.* **2005**, *32*, 1089.
[26] K. Q. Zhao, Y. F. Bai, P. Hu, B. Q. Wang, Y. Shimizu, *Mol. Cryst. Liq. Cryst. Sci.* **2009**, *509*, 77.
[27] Q. L. Hao, X. G.Xie, W. Lei, M. Z. Xia, F. Y. Wang, X. Wang, *J. Phys. Chem. C* **2010**, *114*, 9608.
[28] M. E. Peover, B. S. White, *J. Electroanal. Chem.* **1967**, *13*, 93.
[29] J. Bargon, S. Mohmand, R. J. Waltman, *IBM J. Res. Develop.* **1983**, *27*, 330.
[30] N. M. Yamada, R. B. Kaner, E. W. Chang, in *Electrical and optical polymer systems*, Vol. *3*, (Ed: D. L. Wise), CRC Press, Lancaster, UK **1998**, Ch. 1.
[31] M. Saleh, M. Baumgarten, A. Mavrinskiy, T. Schäafer, K. Müllen, *Macromolecules* **2010**, *43*, 137.
[32] T. S. Qin, G. Zhou, H. Scheiber, R. E. Bauer, M. Baumgarten, C. E. Anson, E. J. W. List, K. Müllen, *Angew. Chem. Int. Ed.* **2008**, *47*, 8292.
[33] V. Bhalla, H. Singh, M. Kumar, *Org. Lett.* **2010**, *12*, 628.
[34] S. Marguet, D. Markovitsi, P. Millié, H. Sigal, *J. Phys. Chem. B* **1998**, *102*, 4697.
[35] D. Markovitsi, A. Germain, P. Millié, P. Lécuyer, L. K. Gallos, P. Argyrakis, H. Bengs, H. Ringsdorf, *J. Phys. Chem.* **1995**, *99*, 1005.
[36] Z. R. Shen, M. Yamada, M. Miyake, *J. Am. Chem. Soc.* **2007**, *129*, 14271.
[37] W. Q. Zhou, H. P. Peng, J. K. Xu, H. Y. Xia, S. Z. Pu, *Polym. Int.* **2008**, *57*, 92.
[38] G. W. Lu, G. Q. Shi, *J. Electroanal. Chem.* **2006**, *586*, 154.
[39] G. W. Lu, L. T. Qu, G. Q. Shi, *Electrochim. Acta* **2005**, *51*, 340.
[40] S. C. Ng, J. M. Xu, H. S. O. Chan, *Macromolecules* **2000**, *33*, 7349.
[41] N. R. Chiou, A. J. Epstein, *Adv. Mater.* **2005**, *17*, 1679.
[42] N. R. Chiou, A. J. Epstein, *Synth. Met.* **2005**, *153*, 69.
[43] B. S. Ong, Y. L. Wu, P. Liu, S. Gardner, *J. Am. Chem. Soc.* **2004**, *126*, 3378.
[44] D. J. Liu, S. De Feyter, P. C. M. Grim, T. Vosch, D. Grebel-Koehler, U.-M. Wiesler, A. J. Berresheim, K. Müllen, F. C. De. Schryver, *Langmuir* **2002**, *18*, 8223.
[45] A. Ajayaghosh, V. K. Praveen, *Acc. Chem. Res.* **2007**, *40*, 644.
[46] Y. Pang, J. Li, T. J. Barton, *J. Mater. Chem.* **1998**, *8*, 1687.
[47] C. A. Parker, T. A. Joyce, *Trans. Faraday Soc.* **1966**, *62*, 2785.
[48] *Handbook of Fluorescence Spectra of Aromatic Molecules*, (Ed: I. B. Berlman), Academic Press, New York **1971**, Ch.1.
[49] D. L. Kokkin, N. J. Reilly, T. P. Troy, K. Nauta, T. W. Schmidt, *J. Chem. Phys.* **2007**, *126*, 084304.
[50] H. Bai, C. Li, G. Q. Shi, *Sens. Actuators B* **2008**, *130*, 777.
[51] S. J. Toal, W. C. Trogler, *J. Mater. Chem.* **2006**, *16*, 2871.
[52] M. E. Germain, M. J. Knapp, *Chem. Soc. Rev.* **2009**, *38*, 2543.
[53] L. Basabe-Desmonts, D. N. Reinhoudt, M. Crego-Calama, *Chem. Soc. Rev.* **2007**, *36*, 993.
[54] S. W. Thomas III, G. D. Joly, T. M. Swager, *Chem. Rev.* **2007**, *107*, 1339.
[55] H. Sohn, M. J. Sailor, D. Magde, W. C. Trogler, *J. Am. Chem. Soc.* **2003**, *125*, 3821.
[56] J. C. Sanchez, A. G. DiPasquale, A. L. Rheingold, T. C. Trogler, *Chem. Mater.* **2007**, *19*, 6459.
[57] H. Sohn, R. M. Calhoun, M. J. Sailor, W. C. Trogler, *Angew. Chem. Int. Ed.* **2001**, *40*, 2104.
[58] J. R. Lakowicz, G. Weber, *Biochemistry* **1973**, *12*, 4161.
[59] L. P. Heng, X. Y. Wang, Y. Q. Dong, J. Zhai, B. Z. Tang, T. X. Wei, L. Jiang, *Chem.- Asian J.* **2008**, *3*, 1041.
[60] J. Q. Wang, L. Huang, M. Xue, Y. Wang, L. Gao, J. H. Zhu, Z. G. Zou, *J. Phys. Chem. C* **2008**, *112*, 5014.
[61] D. P. Kennedy, C. M. Kormos, S. C. Burdette, *J. Am. Chem. Soc.* **2009**, *131*, 8578.
[62] Y. Z. Liao, X. G. Li, R. B. Kaner, *ACS Nano* **2010**, *4*, 5193.

© 2012 WILEY-VCH Verlag GmbH & Co. KGaA, Weinheim